Supplementary Information (SI) for Journal of Materials Chemistry C.

Next-Generation Fluorescent Chemosensor for Dual-Mode Detection of Aluminium Ions and DCP: A Bridge Between Sensing and Bio-imaging

Saurabh Gupta[a§], Abhishek Kaundal[b§], Gulshan Kumar[c], Vijay Luxami[b]*, Kamaldeep Paul[a,b]*

[a]TIET-VT, Centre of Excellence in Emerging Materials, Thapar Institute of Engineering and Technology, Patiala, Punjab, India-147004

[b]Department of Chemistry and Biochemistry, Thapar Institute of Engineering and Technology,

Patiala-147001, India

[c]Department of Chemistry, Banasthali University, Banasthali Newai 304022, Rajasthan, India

*Email: kpaul@thapar.edu , vluxami@thapar.edu

§ Equally Contributed

Materials and methods

Binding constant and limit of detection

The binding constants were determined with Benesi-Hildebrand equation, and the limit of detections were calculated with the help of a standardized IUPAC equation.

$$\frac{1}{I - I_o} = \frac{1}{K_a\,(I_{max} - I_o)[C]^n} + \frac{1}{I_{max} - I_o}$$

Where,

I_o = Intensity of probe in the absence of analyte
I = Intensity of probe at an intermediate analyte concentration

I_{max} = Intensity of probe at a saturation

C = Concentration of analyte,

K_a= Binding constant

The detection limit (DL) was calculated from the following equation:

$$DL = \frac{3 \times standard\ deviation\ of\ blank\ solution}{slope\ of\ calibration\ curve}$$

Quantum Yield

We have calculated the fluorescence quantum yield of **BINNA** in the absence and presence of Al^{3+} ions and DCP using fluorescein as a standard, with a quantum yield of 0.54 (0.1M H_2SO_4) and phenanthrene with a quantum yield of 0.13 (cyclohexane). The formula used is as follows

$$\Phi_S = \Phi_R \times \frac{A_S}{A_R} \times \frac{(Abs)_R}{(Abs)_S} \times \frac{\eta_S}{\eta_R}$$

Where Φ_S is the quantum yield of sample to be tested, Φ_R is the quantum yield of the fluorescein; A_S and A_R are the emission band areas of tested sample and fluorescein, $(Abs)_S$ and $(Abs)_R$ are the maximum absorbance values of the tested sample and fluorescein; η_S and η_R are the refractive index of the solvent used for the sample and fluorescein to record emission band.

Sample preparation for DLS studies

The prepared stock solution was filtered to remove the suspended particles with the help of 0.02 μM filter. Zeta potential analyser (ZEN 3600) was used for conducting DLS experiment. The solution having a concentration of 20 μM was prepared to determine the hydrodynamic size of the particles.

Field Emission-Scanning Electron Microscopy (FE-SEM) measurement

The effect of aggregation has been explored by measuring the changes in particle size and surface morphology using FE-SEM imaging. The **BINNA** solution was placed on a cover slip by drop cast method and allowed to dry for 24 h. The dried sample was subsequently plated with gold spray and FE-SEM analysis was performed. ZEISS MERLIN Compact FE-SEM was used to perform the experiment.

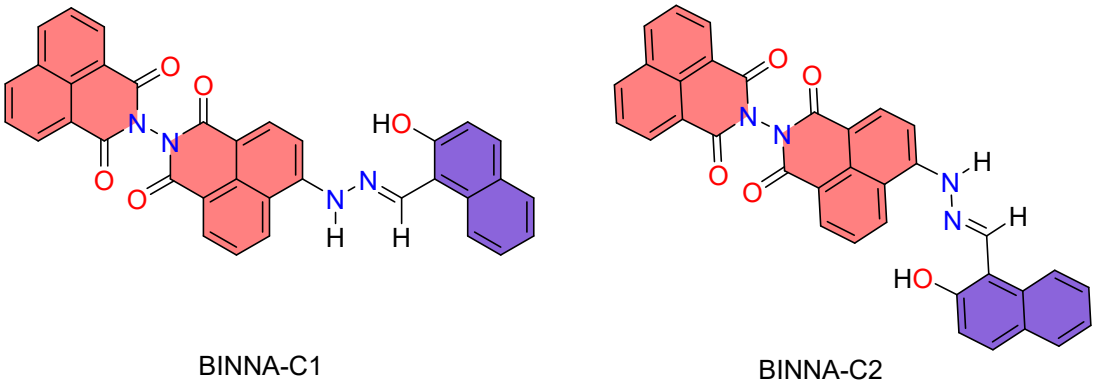

Figure S1: Possible conformations of probe **BINNA**

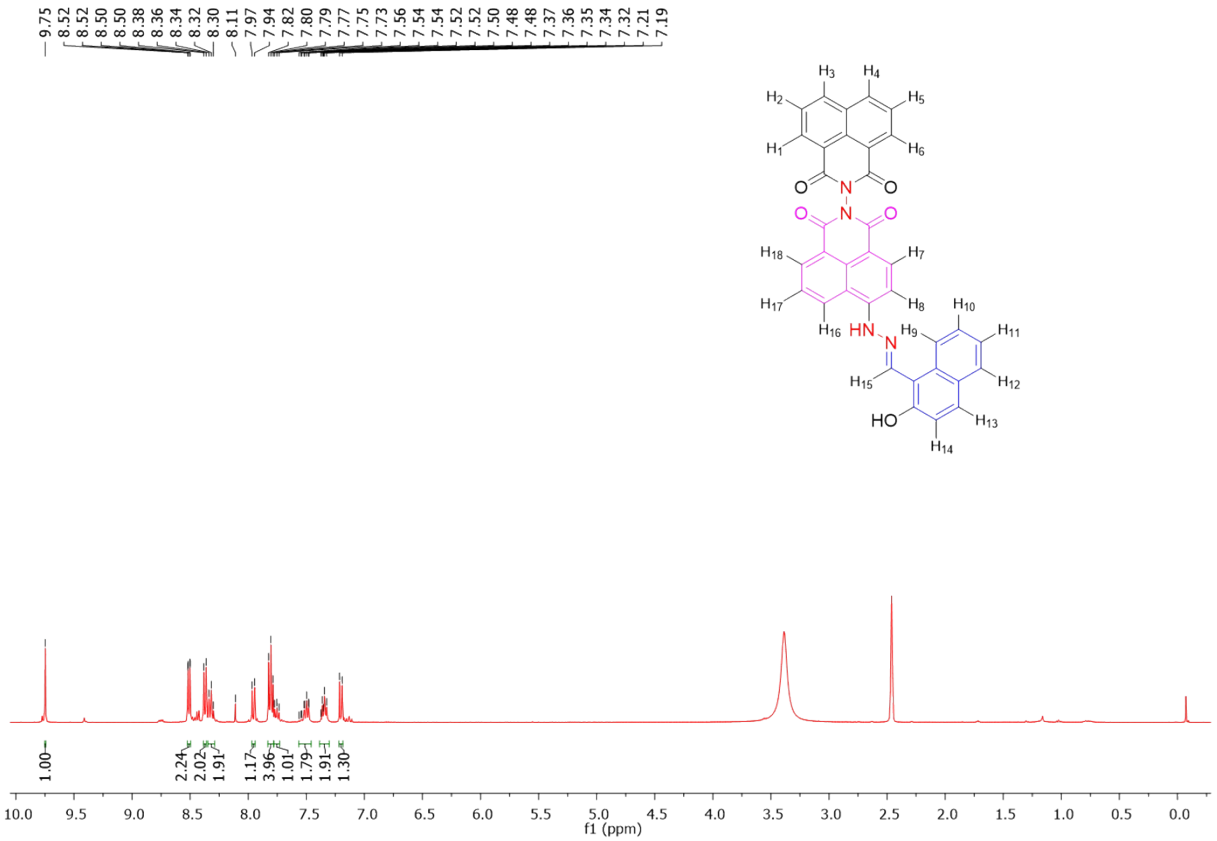

Figure S2: ^{1}H NMR spectrum (DMSO-d_6) of (*E*)-6-(2-((2-hydroxynaphthalen-1-yl)methylene)hydrazinyl)-1*H*,1'*H*,3*H*,3'*H*-[2,2'-bibenzo[*de*]isoquinoline]-1,1',3,3'-tetraone

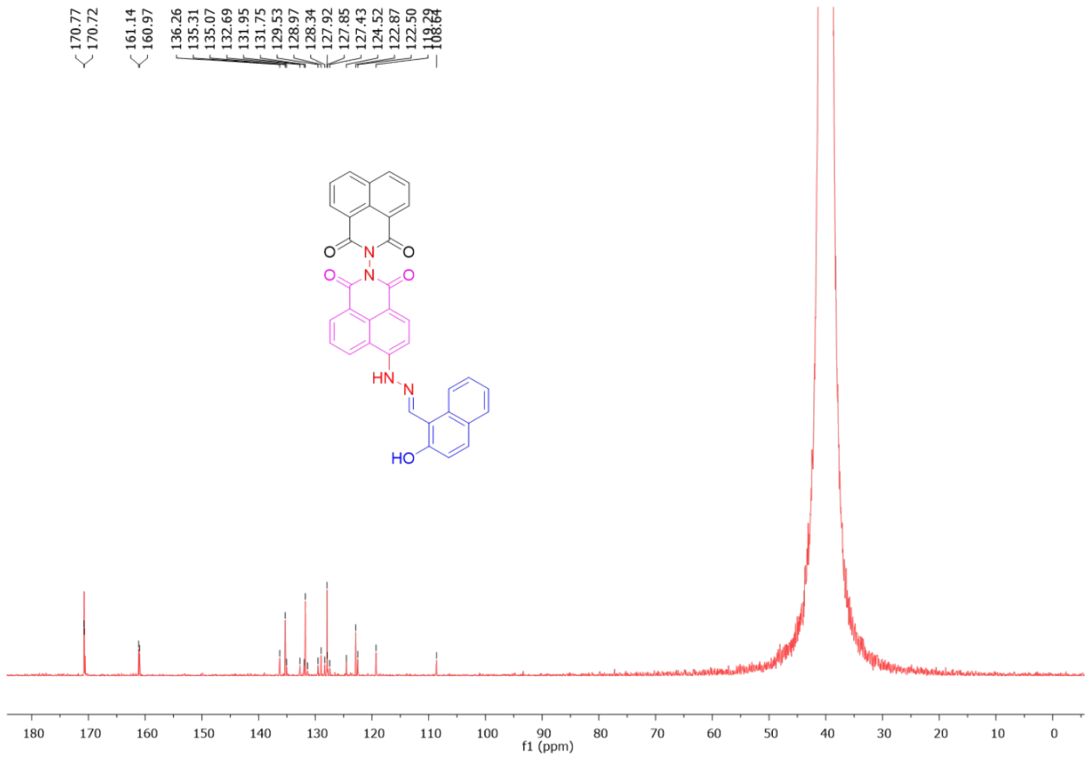

Figure S3: ^{13}C NMR spectrum (DMSO-d_6) of (*E*)-6-(2-((2-hydroxynaphthalen-1-yl)methylene)hydrazinyl)-1*H*,1'*H*,3*H*,3'*H*-[2,2'-bibenzo[*de*]isoquinoline]-1,1',3,3'-tetraone

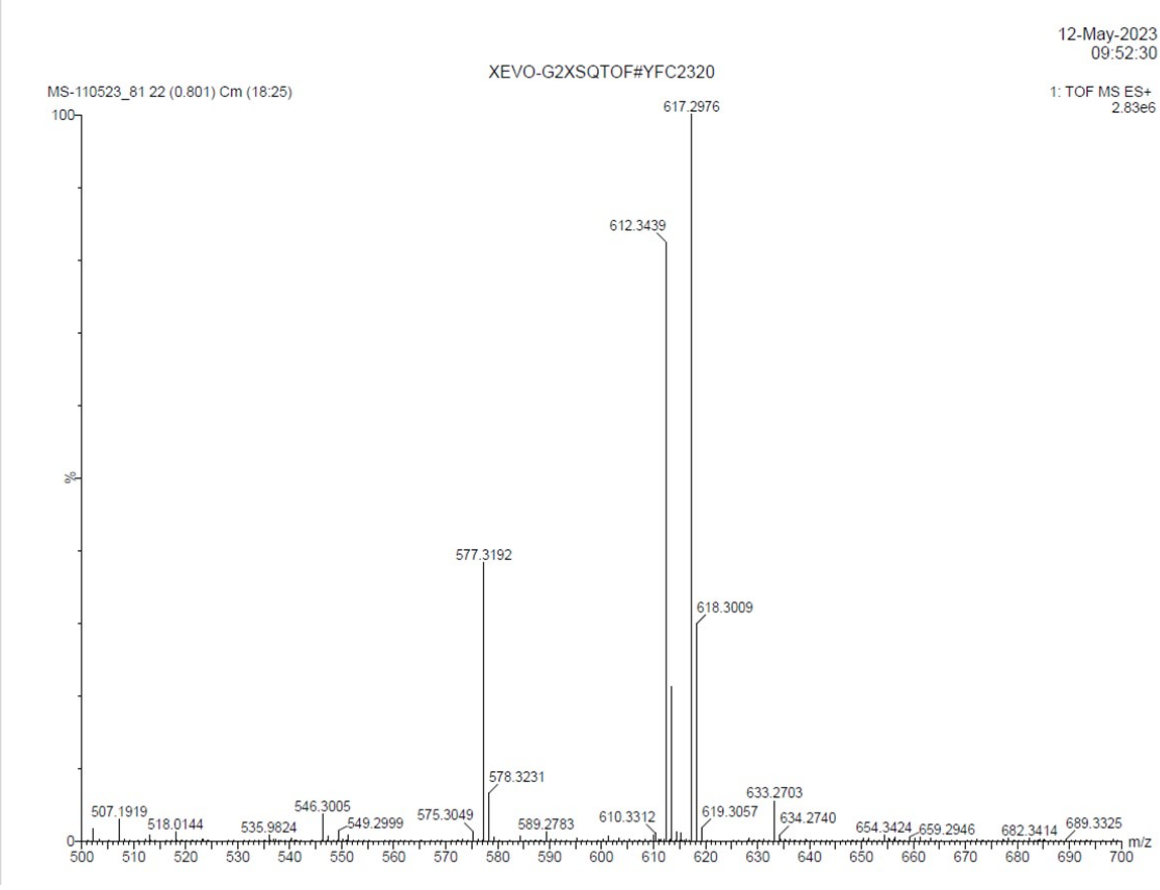

Figure S4: HRMS spectrum of **BINNA**

Efficiency of BINNA

BINNA effectiveness and efficacy in detecting Al^{3+} ions and DCP were contrasted with those of previously published Al^{3+} and DCP sensors (**Table S1**). Based on this data, it is evident that **BINNA** offers a number of benefits over the reported sensors, as it can detect both Al^{3+} and DCP, including a "Turn-On" sensor with better detection limits compared to other reported chemosensors.

Table S1: Comparison of the present sensor with known sensors

S. No.	Sensor	Solvent System	Ion Detected	LOD	Application	Ref
1	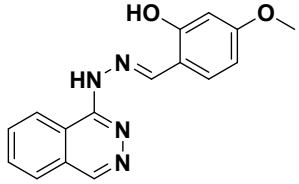	H_2O	Al^{3+}	0.022 µM	Flexible and foldable film	1
2	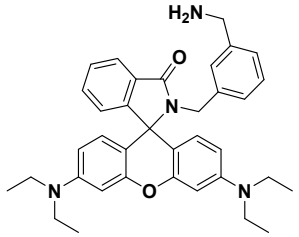	C_2H_5OH:H_2O (7:3)	Al^{3+}	0.098 µM	Test strip and Logic gates	2
3	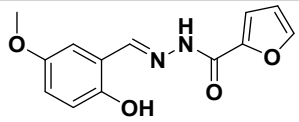	HEPES buffer	Al^{3+}	0.082 µM	Test strip	3
4	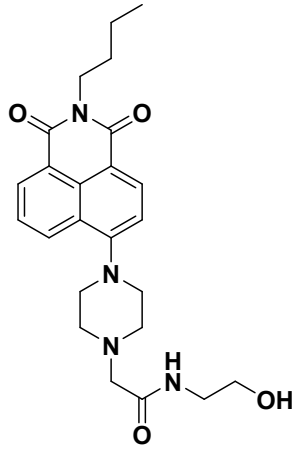	MeOH	Al^{3+}	0.15 µM	Test strip and logic gates	4

5	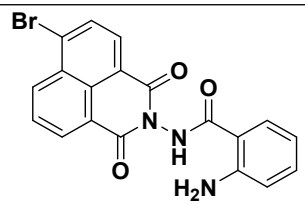	DMSO:H_2O (1:1 v/v)	Al^{3+}	15.2 μM	Cell imaging	5
6	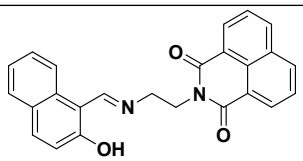	DMSO:H_2O (1:1 v/v)	Al^{3+}	0.033 µM	Pharmaceutical samples	6
7	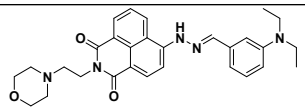	MeOH	Al^{3+}	0.79 μM	Cell imaging and smartphone	7
8	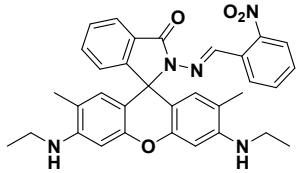	CH_3CN:HEPES (1:1 v/v)	Al^{3+}	1.88 μM	Cell imaging	8
9	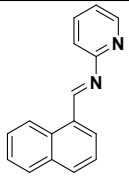	THF:H_2O (1:1 v/v)	Al^{3+}	3.15μM	Real Sample analysis and bioimaging	9
10	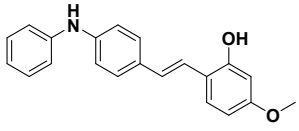	MeOH: HEPES (6:4)	Al^{3+}	12.6 μM	Smartphone and test kit	10
11	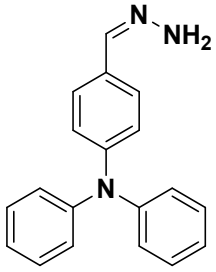	$CHCl_3$	DCP	23.31 nM	Test strip and Bioimaging	11
12	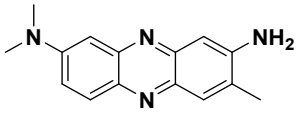	CH_3CN	DCP	0.36 µM	Real Sample analysis	12

13	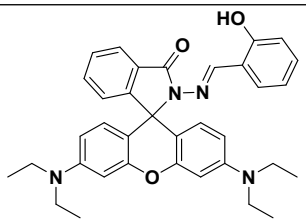	DMSO:H_2O (6:4)	DCP	0.16 µM	Paper strip, smartphone analysis	13
14	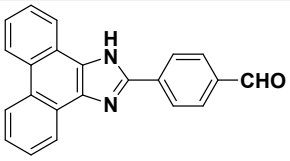	DMSO	DCP	7.4 µM	Smartphone and paper strip	14
15	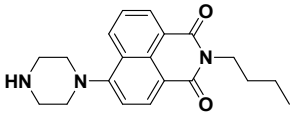	DMF	DCP	5.5 nM	Paper strip	15
16	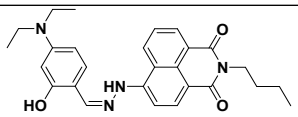	CH_3CN	DCP	1.54 µM	Paper strip	16
17	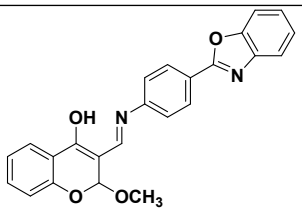	DMSO:H_2O (1:1)	DCP	0.36 µM	Paper strip	17
18	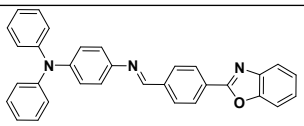	DMSO	DCP	0.42 µM	Paper strip and Real sample analysis	18
19	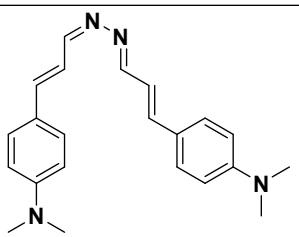	CH_3CN	DCP	0.3 µM	Test strip and real sample analysis	19
20	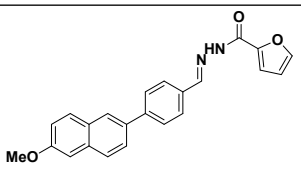	CH_3CN:H_2O (9:1)	DCP	12.2 nM	Paper Strip	20

21	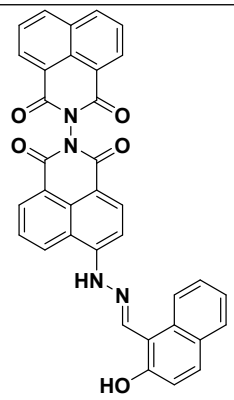	**MeOH**	**Al^{3+}, DCP**	**18.2 nM (0.0182 µM) and 8.5 nM (0.008 µM)**	**Cell Imaging, Logic gate, Real sample analysis**	**This work**

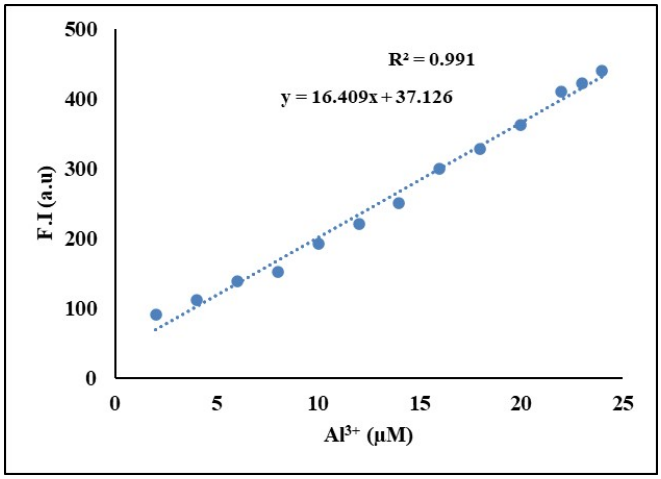

Figure S5: Determination of limit of detection for **BINNA** towards Al^{3+} ions.

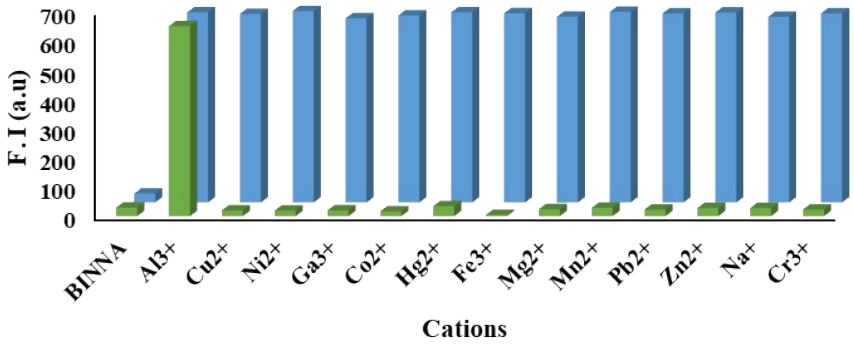

Figure S6: The relative intensity of **BINNA** at 450 nm in the presence and absence of Al^{3+} ions (10 μM), while considering various competing metal ions (50 μM). The change in emission intensity of **BINNA** with different metal ions was represented by green bars, whereas blue bars represent the changes in emission intensity of **BINNA** in the presence of Al^{3+} ions and different competing ions

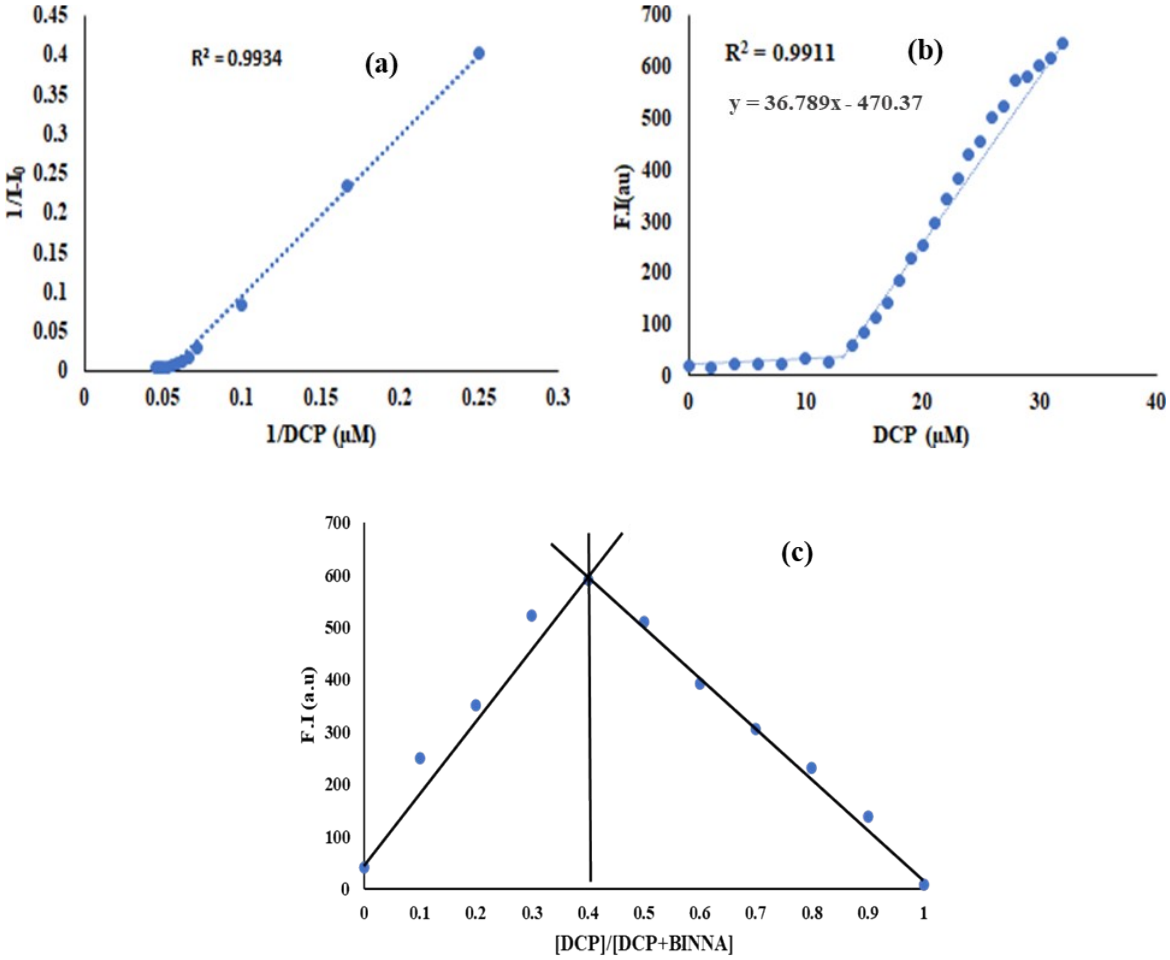

Figure S7: (a) Calculation of binding constant for **BINNA** towards DCP using the Benesi-Hildebrand equation, (**b**) Determination of limit of detection for **BINNA** towards DCP ions. (**c**) Job's plot for calculating the stoichiometry of **BINNA** and DCP using fluorescence spectra.

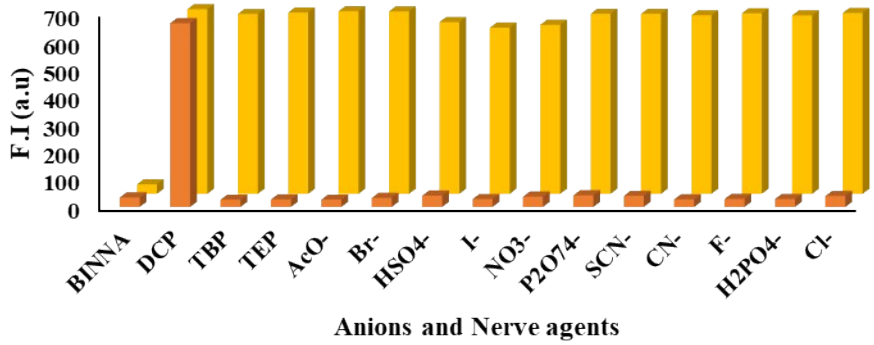

Figure S8: Relative intensity of **BINNA** at 371 nm in the presence and absence of DCP (10 µM) with several anions (50 µM). The fluorescence intensity change of **BINNA** with different anions and nerve agents is represented by orange bars, and yellow bars represent **BINNA**-DCP in the presence of different competing ions and nerve agents.

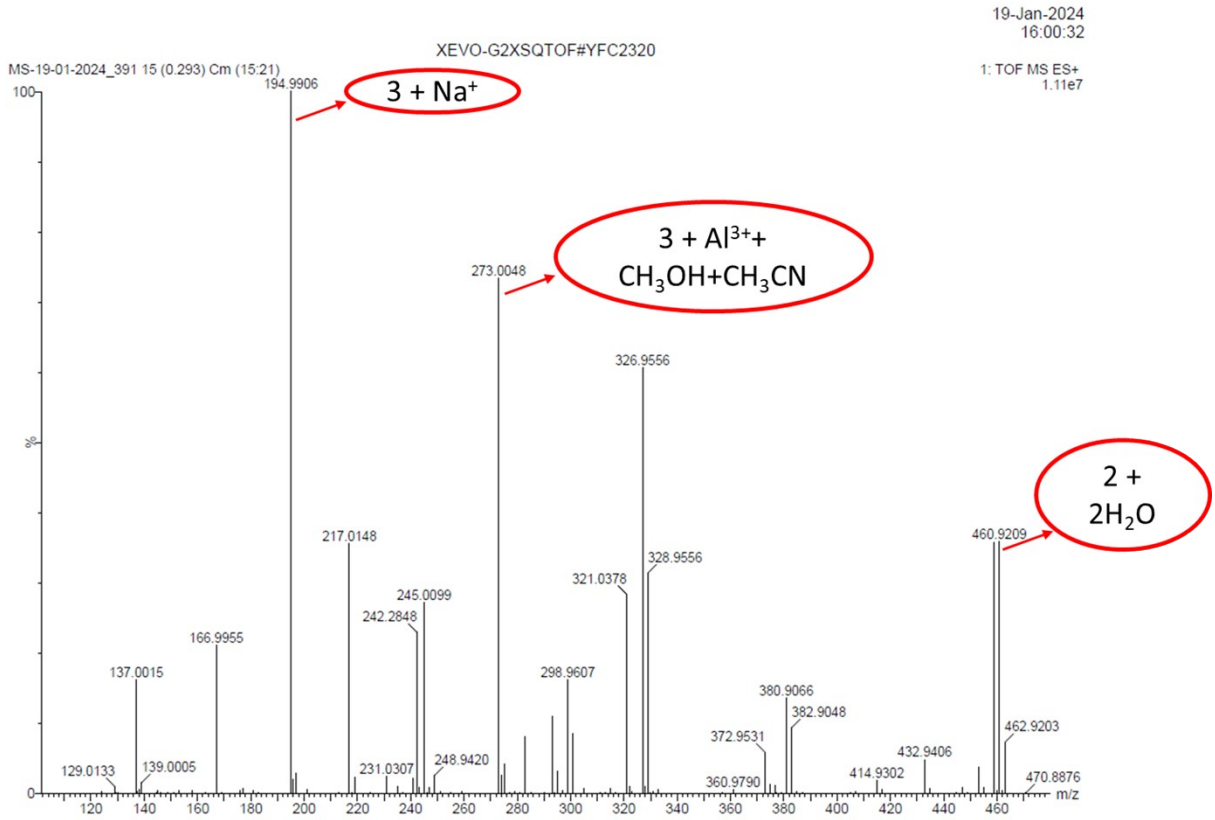

Figure S9: HRMS spectrum of **BINNA** in the presence of Al^{3+} ions

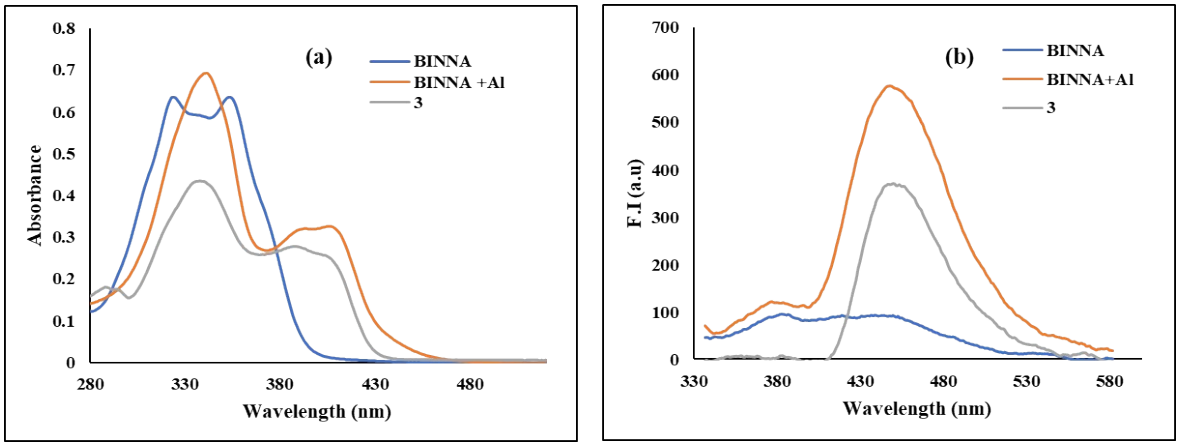

Figure S10: (a) Absorption and (b) emission spectra of **BINNA**, **BINNA**+Al^{3+} and **3**

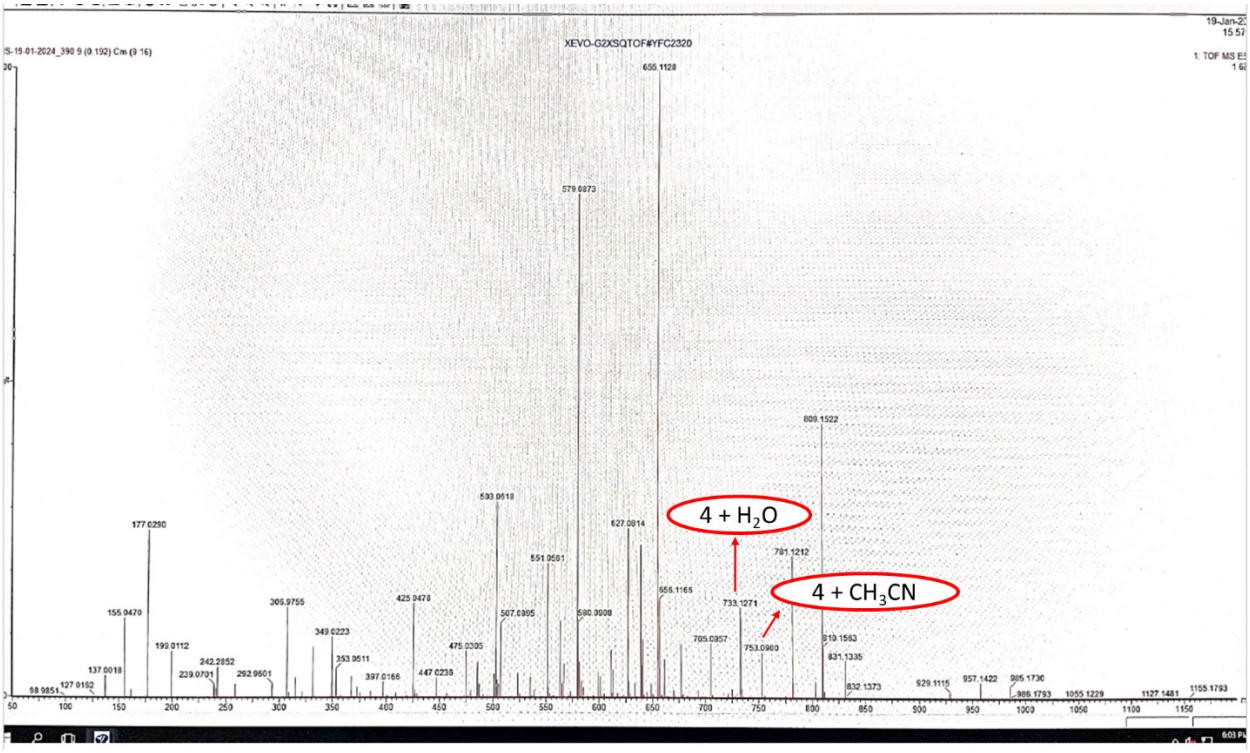

Figure S11: HRMS spectrum of **BINNA** in the presence of DCP

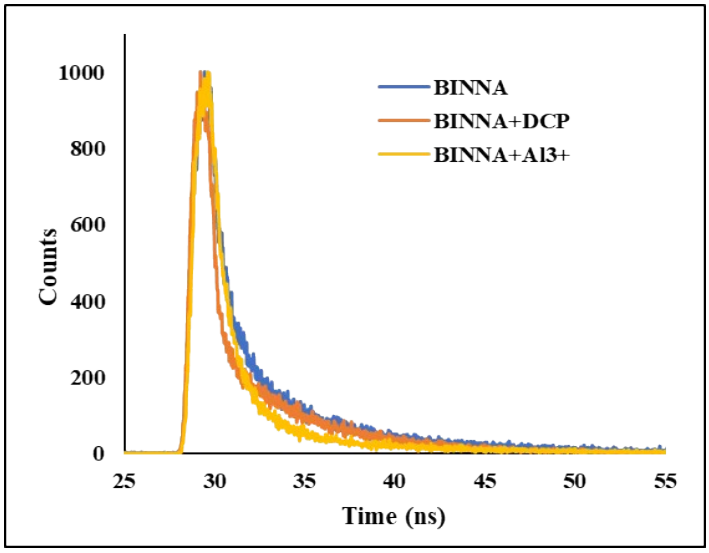

Figure S12: Time-resolved spectra of **BINNA** (CH_3OH) in the absence and presence of DCP and Al^{3+} ions.

Table S2: Calculated electronic spectra of **BINNA** in different solvents

		Absorption peak (λ; nm)	**Oscillation strength (f)**	**Dipole moment (a.u.)**
Solvents	Chloroform	392	1.1576	4.52
	MeOH	397	1.1692	5.33
	DMSO	399	1.1854	5.38
	Acetone	393	1.1418	4.96

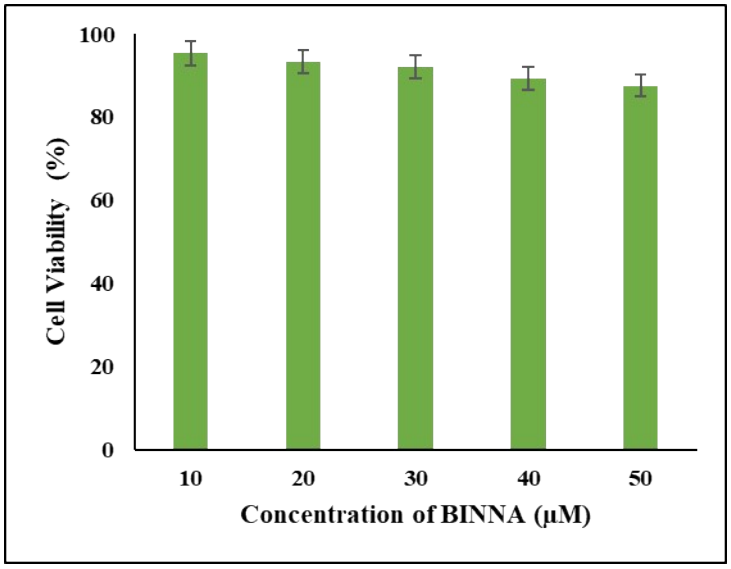

Figure S13: Cell viability of *E. coli* cells incubated with **BINNA** with different concentration (10, 20, 30, 40 and 50 µM) for 24h

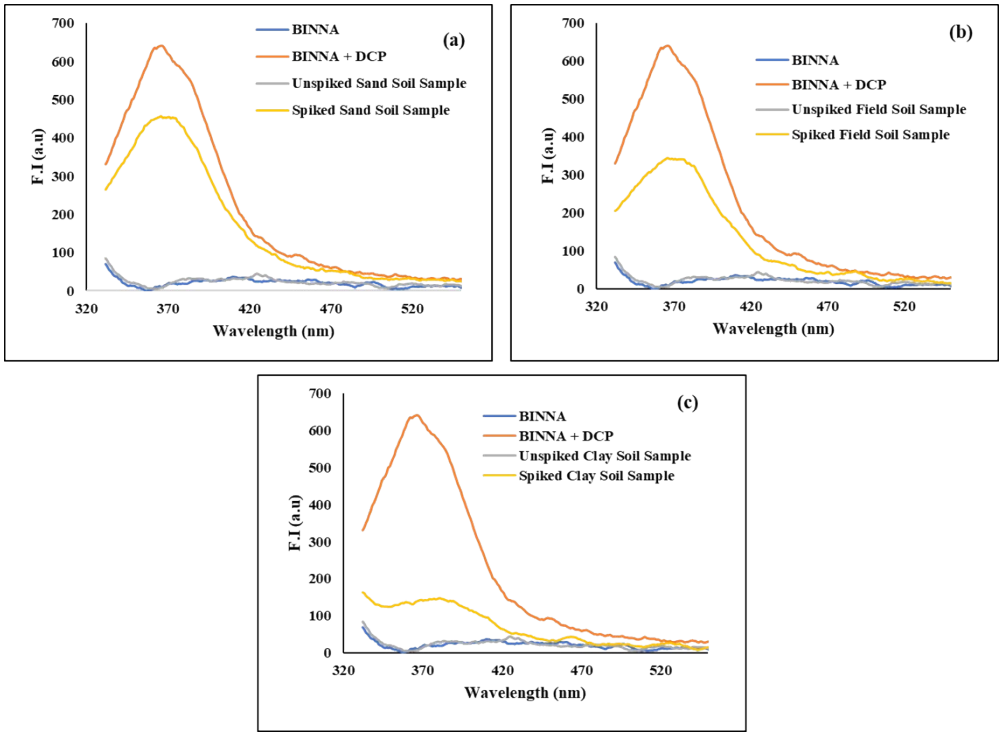

Figure S14: Emission spectra of **BINNA** solution in different spiked and unspiked DCP soil samples such as (a) sand, (b) field, and (c) clay soil.

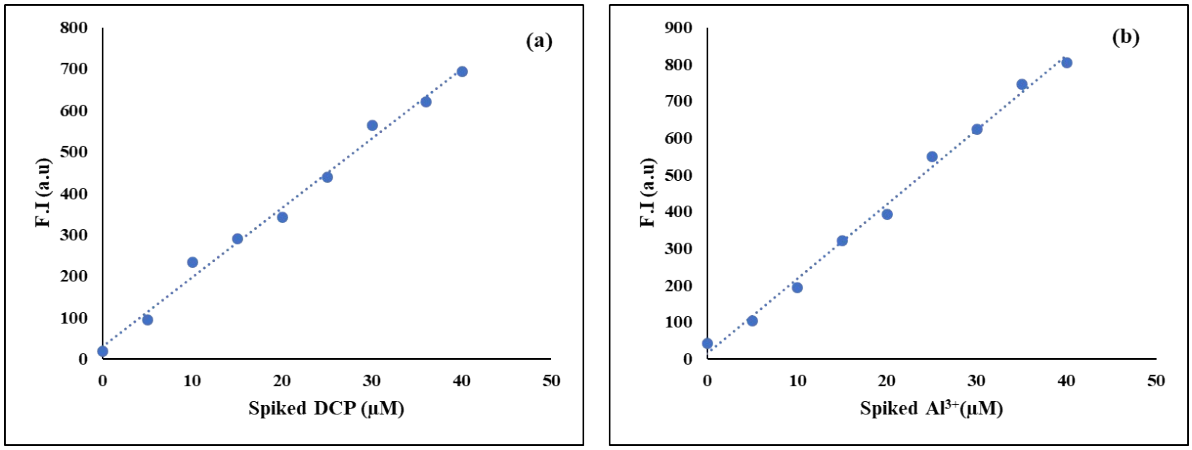

Figure S15: Calibration curve for (a) DCP and (b) Al^{3+} ions.

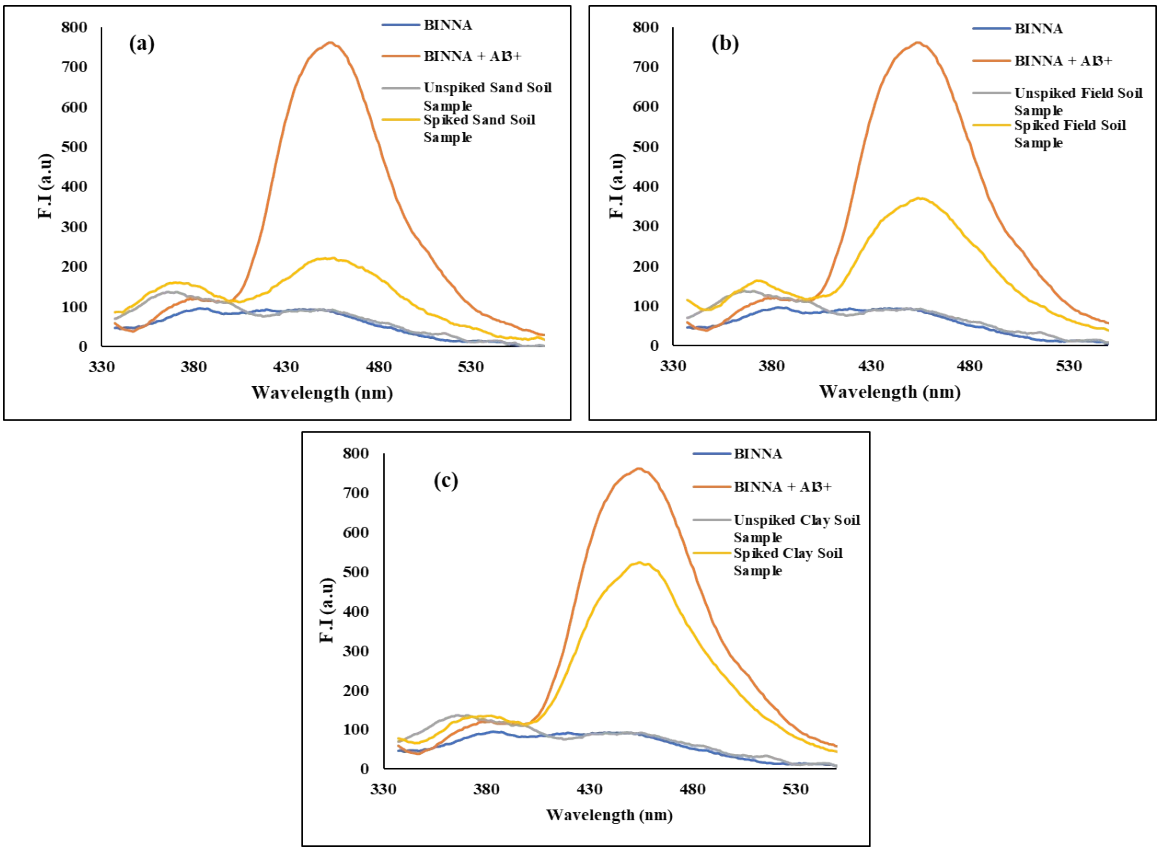

Figure S16: Emission spectra of **BINNA** solution in different Al^{3+} spiked and unspiked soil samples such as (a) sand, (b) field, and (c) clay soil

References

1. Yang, Y. Y.; Ma, P. Y.; Xue, J. H.; Yang, D. D.; Shi, Y. S.; Zhao, X.; Ma, Q. A Highly Selective Fluorescent Probe Based on Multi-Binding Site Hydrazone Chemosensor for Al^{3+} Detection. *Microchem. J.* **2024**, *200*, 110495.

2. Biswal, B.; Bihari Bhoi, B.; Charan Behera, K.; Khamari, U.; Bag, B. A Rhodamine B Based Chemosensor for Selective Detection of Al^{3+} Ion: Photophysical Investigations and Analysis in Real Samples. *Inorg. Chim. Acta* **2024**, *571*, 122225.
3. Shaikh, A.; Shaikh, J.; Ansari, D.; Sheikh, K. N.; Tambe, P.; Shaikh, S.; Lande, D. N.; Gejji, S. P.; Ahmed, K. A 'Turn-on' Fluorescence Sensor Based on 5-Methoxy Salicylaldehyde Hydrazone for Selective Detection of Al^{3+} Ions. *J. Mol. Struct.* **2025**, *1328*, 141317.
4. Li, N. N.; Zeng, S.; Li, M. Q.; Ma, Y. Q.; Sun, X. J.; Xing, Z. Y.; Li, J. L. A Highly Selective Naphthalimide-Based Chemosensor: "Naked-Eye" Colorimetric and Fluorescent Turn-On Recognition of Al^{3+} and Its Application in Practical Samples, Test Paper and Logic Gate. *J. Fluoresc.* **2018**, *28*, 347–357.
5. Anand, T.; Ashok Kumar, S. K.; Sahoo, S. K. A New Al^{3+} Selective Fluorescent Turn-on Sensor Based on Hydrazide-Naphthalic Anhydride Conjugate and Its Application in Live Cells Imaging. *Spectrochim. Acta - Part A Mol. Biomol. Spectrosc.* **2018**, *204*, 105–112.
6. Saha, S.; Mondal, S.; Sahoo, P. Fabrication of a Luminescent Chemosensor for Selective Detection of Al^{3+} Used as an Adjuvant in Pharmaceutical Drugs. *Org. Biomol. Chem.* **2022**, *21*, 981–986.
7. Zhang, Q.; Zhang, D.; Shi, Z.; Jin, C.; Jiang, Y. Construction of Naphthalimide-Based Fluorescent Probe for Sequential Detection of Al^{3+} and NOR and Its Application in Tea and Honey. *Spectrochim. Acta - Part A Mol. Biomol. Spectrosc.* **2025**, *330*, 125685.
8. Gauthama, B. U.; Narayana, B.; Sarojini, B. K.; Srijana, P. J.; Kodlady, S. N.; Sangappa, Y.; Kudva, A. K.; Raghu, S. V. A Hybrid Fluorescent Probe for the Selective Detection of Divalent Hg^{2+} and Trivalent Al^{3+} Ions and Their Biological Applications. *Results Chem.* **2024**, *8*, 101591.
9. Suresh, S.; Prabakaran, G.; Prabhu, J.; Vijayanand, P. S.; Kumar, R. S.; Karthick, R.; Velraj, G.; Nandhakumar, R. A Pyridine Naphthalene Conjugate: ESIPT Based Molecular Chemosensor for Al^{3+} Ions and Sequential Detection of H_2PO^{4-} and Applications in Milk, Water Samples and Bio-Imaging. *J. Food Compos. Anal.* **2024**, *132*, 106364.
10. Guctekin Yasar, O.; Karuk Elmas, S. N.; Aydin, D.; Arslan, F. N. Al^{3+} Selective Ratiometric Fluorescent and Colorimetric Chemoprobe and Its Practical Applications in Foods, Test Kits and Smartphone. *J. Photochem. Photobiol. A Chem.* **2024**, *447*, 115238.

11. AbhijnaKrishna, R.; Wu, S. P.; Velmathi, S. On-Spot Detection of Diethylchlorophosphate through Device Fabrication, Pen and Spray Method Based on Intramolecular Charge Transfer Modulated Sensor Molecule Extending Application to Cell Imaging. *Microchem. J.* **2024**, *205*, 111369.
12. Sarkar, P.; Tohora, N.; Mahato, M.; Ahamed, S.; Sultana, T.; Das, S. K. A Selective Chromo-Fluorogenic Chemosensor for Visual Detection of Solution and Vapor Phase of Sarin, Tabun Mimics Diethyl Chlorophosphate, Diethyl Cyanophosphonate. *J. Mol. Struct.* **2024**, *1306*, 137846.
13. Tohora, N.; Ahamed, S.; Mahato, M.; Sultana, T.; Chourasia, J.; Maiti, A.; Das, S. K. Highly Specific and Sensitive Chromo-Fluorogenic Detection of Sarin, Tabun, and Mustard Gas Stimulants: A Multianalyte Recognition Approach. *Photochem. Photobiol. Sci.* **2024**, *23*, 763–780.
14. Sultana, T.; Mahato, M.; Tohora, N.; Ahamed, S.; Maiti, A.; Das, S. K. A Phenanthroimidazole-Based Luminophore for Selective and Specific Identification of Sarin Simulant, Diethylchlorophosphate. *J. Fluoresc.* **2024**, 1625–1636.
15. Xu, H.; Zhang, H.; Zhao, L.; Peng, C.; Liu, G.; Cheng, T. A Naphthalimide-Based Fluorescent Probe for the Highly Sensitive and Selective Detection of Nerve Agent Mimic DCP in Solution and Vapor Phase. *New J. Chem.* **2020**, *44*, 10713–10718.
16. Jain, N.; Kaur, N. Smartphone Coupled, Solution, Solid and Vapour Phase Sensing of Nerve Agent Mimic by 1,8-Naphthalimide Derived Schiff Base. *Results Opt.* **2023**, *12*, 100466.
17. Sultana, T.; Mahato, M.; Ahamed, S.; Tohora, N.; Chourasia, J.; Ali, S.; Das, S. K. A Highly Selective Chromo-Fluorogenic Probe for Specific Detection of Sarin Gas Simulant Diethylchlorophosphate in Liquid and Vapor Phases. *Sens. Diagn.* **2024**, *3*, 1285–1297.
18. Sultana, T.; Mahato, M.; Tohora, N.; Ahamed, S.; Maiti, A.; Ghanta, S.; Das, S. K. A Benzoxazole-Triphenylamine Conjugated Fluorogenic Probe for Specific Detection of Sarin Gas Mimic Diethylchlorophosphate. *Anal. Methods* **2024**, *16*, 759–771.
19. Mahato, M.; Sultana, T.; Maiti, A.; Ahamed, S.; Tohora, N.; Ghanta, S.; Das, S. K. Highly Selective and Sensitive Chromogenic Recognition of Sarin Gas Mimicking Diethylchlorophosphate. *Anal. Methods* **2024**, *16*, 1371–1382.
20. Banerjee, S.; Ghosh, P.; Karak, A.; Banik, D.; Mahapatra, A. K. A Chemodosimetric Chemosensor for the Ratiometric Detection of Nerve Agent-Mimic DCP in Solution and Vapor Phases. *Anal. Methods* **2024**, 432–439.